# The effects of wide incidence angles on crosswell reflection imaging

Joongmoo Byun

James Ward Rector III

Department of Materials Science and Mineral Engineering

University of California at Berkeley

**ABSTRACT**

Three effects related to the wide incidence angles in crosswell reflection imaging, phase shift at post-critical incidence angles, in-plane Fresnel zone effect, and wave stretch in image, were investigated separately with model studies. To isolate the above effects, crosswell data were modeled with both a ray tracing and a finite difference approach based on the acoustic wave equation. Phase shifts occur at post-critical incidence angles degrading the stacked (over incidence angle) reflection image. The Fresnel zone effect produces a misalignment of the wavelet peak without the phase shift. However, these misalignments do not degrade the stack quality significantly compared with the post-critical incidence angle effect. The wavelet stretch effect produced in the imaging operation (mapping or migration) broadens the bandwidth of the stacked reflections, but it also introduces a vertically and laterally variable wavelet due to the variable reflection incidence angle coverage of each stacked trace. To remove the wavelet stretch effect, we applied spectral shaping, which compensates for wavelet stretch by applying a bandpass filter with the same range to all traces in the stacked section and whitens the wavenumber spectra.

**KEY WORDS:** crosswell, wide incidence angle, post-critical angle, Fresnel zone, stretch effect.

## INTRODUCTION

The application of the crosswell seismic reflection method to reservoir characterization and monitoring of enhanced oil recovery processes has recently become widespread (e.g. Harris, et al., 1995, Sheline, 1995, Langan, et al., 1998). However, the reflection incidence angles utilized in crosswell seismic data are wider (typically between 40° ~ 80°) than those used in conventional surface seismic (typically less than 30°). There are a number of imaging issues created by using these wide reflection incidence angles. Besides the well-known amplitude variation with incidence angle (called AVO in surface seismic), phase and frequency modulation of imaged reflections can also occur at very wide angles. These issues do not occur only in crosswell seismic geometry, but also can occur in long-offset VSP and surface seismic acquisition when source/receiver offsets are very large. In this paper, we investigate three aspects related to the imaging of wide incidence angles: the presence of incidence angles beyond the critical angle, Fresnel zone effects, and wavelet stretch in the reflection image.

To decompose these three issues into separate imaging problems, we used both ray trace and finite difference modeling, creating synthetic data for the 1-D velocity fields shown in Table 1.

## MODEL GEOMETRY AND MODELING TECHNIQUES

A two-layer structure with horizontal reflection interfaces was used for model studies (Fig. 1). To simulate a crosswell geometry with vertical boreholes, sources were located from 2000 to 2680 ft (from 609.6 to 816.9 m) in depth and receivers were located from 2000 to 2795 ft (from 609.6 to 851.9 m) in depth. Both source and receiver intervals were 5 ft (1.5 m). A zero-phase Ricker wavelet with a center frequency of 700 Hz was used as a source wavelet. The borehole radiation patterns of sources and receivers were not considered in this study, rather, an omnidirectional radiation pattern was assumed. The distance between source and receiver well was 991 ft (302.1 m) and the depth of horizontal reflection interface was 2700 ft (823 m). Three velocity models were created. The velocity of the upper layer was fixed at 6000 ft/s (1828.8 m/s) in all models. In the first model (model 1), the velocity of the lower layer was 8000 ft/s (2438 m/s) to evaluate critical angle effects. In the second model (model 2), the lower layer velocity was 5900 ft/s (1798 m/s), and, in the third model (model 3), the lower layer velocity was 4000 ft/s (1219.2 m). To model the crosswell data, two methods were used. The first method was based on ray tracing and the second method was a finite difference approach based on the acoustic wave equation. With the ray tracing method, we obtained only specular arrivals such as transmitted P or reflected P and did not produce wave phenomena such as Fresnel zone effects or head waves. On the other hand, the acoustic finite difference method produced all acoustic wave phenomena, including head waves and Fresnel zone effects. However, elastic effects such as P-S mode-converted waves were not incorporated. Also, AVO effects and critical angle effects were not accurately represented.

## EFFECTS OF INCIDENCE ANGLE BEYOND THE CRITICAL ANGLE

If a plane P wave strikes obliquely at a horizontal interface, a reflected P wave, a transmitted P wave, and mode-converted waves such as reflected and transmitted S waves are produced. In this situation, the reflection coefficient depends on incidence angle. If the velocity of the upper layer is less than that of the

underlying layer and the incident wave strikes with an angle beyond the critical angle, a phase shift occurs in the reflected arrival.

To investigate only this phenomenon, we used ray tracing, which does not produce a Fresnel zone effect. Using a velocity of 6000 ft/s for the upper layer and 8000 ft/s for the lower layer, post-critical reflections were produced for incidence angles beyond 49°. Figure 2 shows the effects of post-critical reflection incidence angles for the crosswell geometry of Fig. 1. In Fig. 2, the reflected waves are flattened to a constant time (100 ms) using the specular traveltime. When flattened to a constant time by using the specular traveltime, the phase shift effect is obvious. For the traces where the incidence angles are beyond the critical angle, there is a gradual phase delay that increases with increasing incidence angle. This post-critical phase shift will produce a wavelet cancellation in stacking. Therefore, if we stack mapped or migrated data without correcting for the post-critical phase shift, this effect can degrade the benefits of stacking.

To stack the mapped or migrated data, we transform the data into a common-reflection-point (CRP) gather (Lazaratos, 1993). Figure 3 shows the phase shift effect due to the post-critical incidence angle in a common-reflection-point gather (in this case, a point roughly 2/3 of the way between the source and receiver wells). To examine the effect of post-critical phase shift on stacking, we compared phase-corrected and uncorrected root-mean-square amplitudes of the stacked trace with this gather. The width of the time window centered on the datum (100 ms) that was used to calculate RMS amplitude was 4 ms. Stacking was performed with traces in the incidence angle range of 30° ~ 80°, the angle range used commonly in crosswell reflection seismic for stacking. The RMS amplitude obtained from the stacked trace without correction was about 56% of the value obtained from the stacked trace with correction. From the above result, we can see that the correction of the post-critical phase shift effect is necessary to improve stack quality.

**FRESNEL ZONE EFFECTS**

The first Fresnel zone is defined as the portion of a reflector from which reflected energy can reach a detector within one-half wavelength of the specular reflected energy (Sheriff, 1991). The Fresnel zone affects the vertical and lateral resolution of seismic data. In crosswell data, there is an in-plane Fresnel

zone, which was considered in the reflection response from scatters located in the interwell plane, and also an out-of-plane Fresnel zone. While the size of the in-plane Fresnel zone increases with increasing incidence angle, the size of the out-of-plane Fresnel zone decreases with increasing incidence angle (Lazaratos, 1993). Therefore, we consider only the in-plane Fresnel zone in this study. The basic geometry for the in-plane Fresnel zone is shown in Fig. 4. Suppose that the specular reflection point is point A and that t is the reflection traveltime. The isochronal ellipse corresponding to time t+T/2, where T is the dominant period, intersects the horizontal reflector at points B and C. By definition, the in-plane size of the Fresnel zone is the length of the segment BC. Figure 5 shows the size of the in-plane Fresnel zone as a function of the horizontal location of the reflection point and the incidence angle. The in-plane Fresnel zone size is expressed in terms of the fraction of the interwell distance. From this figure, we can see that the size of the in-plane Fresnel zone is smallest at the wells and increases as we move towards the midpoint between the two wells. In other words, the lateral resolution of crosswell reflection data (unmigrated) is highest near the wells and decreases toward the middle of the image. Also, we can observe that the in-plane Fresnel zone effect increases with increasing incidence angle.

A 2-D finite-difference method based on the acoustic wave equation was used to generate the crosswell seismic data for investigation of the in-plane Fresnel zone effect. We used a velocity of 5900 ft/s for the lower layer so that there was no critical angle. The section shown in Fig. 6 is a common-reflection-point (CRP) gather at the same reflection point used in Fig. 3. The reflected waves are flattened to a constant time as was done in the post-critical angle analysis. From the figure, we can see that the in-plane Fresnel zone effect appears as a misalignment of the peak of the wavelet without a phase shift in the image. The time shift of the peak increases by 0.015 ms as the incidence angle increases 1°. The RMS amplitude obtained from the stacked trace without correction was about 83% of the value obtained from the stacked trace with correction. Therefore, the Fresnel zone effect does not significantly degrade the stack quality compared with the post-critical incidence angle effect.

In imaging crosswell reflection data, errors in the imaging velocity produce misalignments of reflectors in a CRP gather. Therefore, the Fresnel zone effect, which also produces a misalignment of a reflector in a crosswell image, can be described as the equivalent of a velocity error in imaging the data. For example, the delay of the wavelet peak from the datum (100 ms) is 0.55 ms for the trace whose incidence angle is

80°. This misalignment value is equivalent to a 3.8% velocity error in VSP-CDP mapping (Lazaratos, 1993). This velocity error is within the reproducibility limits of repeat crosswell tomogram (Langan, personal communication).

**WAVELET STRETCH IN IMAGE**

There are two kinds of common imaging methods for crosswell reflection data. One is VSP-CDP mapping (Lazaratos, 1993), which is a point-to-point transformation similar to the normal moveout (NMO) correction in surface seismic. The other is migration (Mo, et al., 1993, Qin and Schuster, 1993). We used VSP-CDP mapping in our model studies. Since a VSP-CDP mapping algorithm maps traces to curvilinear trajectories, it produces wavelet distortion, similar to the stretch associated with the NMO correction. While a NMO correction produces only vertical stretch, the non-vertical trajectories used in VSP-CDP mapping produces both a vertical and a horizontal stretch. Pre-stack crosswell migration produces a similar stretch effect when the wavefield being used is not propagating parallel to the vertical array of image points (Brown, 1994). Stretch effects are easier to characterize in VSP-CDP mapping than in pre-stack migration because the former is a point-to-point transformation.

The stretch effect in VSP-CDP mapping reduces the wavenumber band of the image wavelet as the incidence angle increases. The effective horizontal and vertical wavelengths due to stretch after VSP-CDP mapping for the constant velocity case are as follows (Lazaratos, 1993):

$$\lambda_x = \left[1 - 2\left(\frac{x}{x_{well}}\right)\right]\frac{\lambda}{2}\frac{\tan\phi}{\cos\phi} \qquad (1)$$

$$\lambda_z = \frac{\lambda}{2\cos\phi} \quad , \qquad (2)$$

where $\lambda_x$ is the horizontal wavelength due to stretch after VSP-CDP mapping, $\lambda_z$ is the vertical wavelength due to stretch after VSP-CDP mapping, $\lambda$ is the wavelength $2\pi v/\omega$, $x_{well}$ is the distance between source and receiver wells, $x$ is the distance of reflection point from the source well, and $\phi$ is the incidence angle.

From the above equations, we can see that vertical and lateral stretch effects increase as the incidence angle increases. In addition, while the vertical stretch is independent of the position of the reflection point, lateral

stretch is largest close to the wells and decreases as the reflection points move towards the middle of the interwell space. The vertical stretch effect appears as a lowering of the central wavenumber, thereby degrading the vertical resolution. Figure 7 shows a common-reflection-point (CRP) gather at the same CRP as that in Fig. 3 after applying VSP-CDP mapping to the model 3 data. The stretch effect related to VSP-CDP mapping increases as the incidence angle increases, and it increases abruptly when the incidence angles are greater than 80°. The large stretch effects related to angles above 80° make it difficult to use these angles for imaging.

The stretch effect in the wavelet appears as a lowering of the central wavenumber and a reduction in the wavenumber bandwidth as shown in Fig. 7. Therefore, the effect of stretch on stacking is a little different from the previous two cases. Figure 8 shows stacked wavelets for different angle ranges along with the wavelets corresponding to the minimum (39°) and maximum incidence angle (80°) used in stacking. As the incidence angle increases, the wavelength of the stacked wavelet increases. However, the main lobe of the stacked wavelet is narrower than the trace corresponding to the 80° incidence angle, even though its dominant wavelength is similar. The spectra in Fig. 9 explain this phenomenon. From these spectra, we see that the main wavenumber moves lower as we use higher incidence angles in stacking. If we compare the spectrum of the 30° ~ 80° stacked wavelet with that of the 80° wavelet, we see that the main wavenumbers of both traces are similar but the stacked trace has greater bandwidth. While the wavelength of the wavelet and the related resolution are determined by its main wavenumber, the width of the wavelet main lobe is controlled by its bandwidth. Therefore, the use of stretched wavelets in stacking narrows the main lobe even though it lowers the main wavenumber. This bandwidth enhancement is a positive effect of wavelet stretch. Bandwidth enhancement due to wavelet stretch is more pronounced in crosswell seismic geometry, because there is a greater incidence angle range than for surface seismic recording.

If there was no stretch effect, the signal wavenumber bands of the traces used in stacking would be identical for all wavenumbers and would be enhanced equally by stacking. However, when a stretch effect exists, the signal wavenumber bands of the traces change with incidence angles. Figure 10a shows the change of the wavenumber band of the wavelet for different incidence angles when we apply VSP-CDP mapping to the model wavelet that has a frequency band of 400 ~ 700 Hz in the time domain. This change of the wavenumber band of the signal makes the stacking fold different for different wavenumbers (Fig.

10b). Therefore, if the noise also has a wide band, the signal-to-noise ratio in the stacked trace varies as a function of wavenumber.

## CORRECTION OF THE STRETCH EFFECT

Spectral shaping can be used to correct for the stretch effect in the VSP-CDP mapped image. If we apply a bandpass filter to all traces in the VSP-CDP mapped section with the same wavenumber range and equalize the wavenumber spectrum, we can create a VSP-CDP mapped image with a uniform wavelet. This approach is similar to the method introduced by Haldorsen and Farmer. (1989) to compensate for the stretch effect due to NMO correction in surface seismic.

Figure 11 shows the result after applying spectral shaping to the CRP gather in Fig. 7 with a wavenumber range of 0.03 ~ 0.01 $ft^{-1}$. Even though the wavelet was wider, we obtained uniform wavelets for incidence angles less than 80°. Since wavelet stretch effect increases abruptly, we failed to correct the stretch effect with spectral shaping for wavelets with incidence angles greater than 80°. The correction of stretch effect with spectral shaping improves the uniformity of the S/N ratio and the resolution in the stacked data when we stack the VSP-CDP mapped data with incidence angles less than 80°.

## CONCLUSIONS

One of the features of crosswell reflection data is the use of large (typically 40° ~ 80°) incidence angles in reflection imaging. These wide incidence angles create complications for reflection imaging such as near- and post-critical angle effects, Fresnel zone effect, and wavelet stretch. These three effects were examined separately with model studies. All three effects become more severe with increasing incidence angle. A phase shift occurs in reflected wavelets with incidence angle beyond the critical angle. This phase shift can cancel the wavelet in stacking and degrade the stacking quality. The Fresnel zone effect produces a misalignment of the wavelet peak without a phase shift. However, the degradation on the stack quality due to this misalignment is less than that due to the phase shift at post-critical incidence angles. A wavelet stretch occurs both vertically and horizontally when we image crosswell reflection data by VSP-CDP mapping or migration. The stretch effect reduces the main wavenumber of the wavelet and creates a narrower wavenumber band with increasing incidence angle. The use of stretched wavelets in stacking

compresses the main lobe of the stacked wavelet and changes the S/N ratio as a function of wavenumber. In addition, the variable reflection angle coverage introduces a laterally and vertically variable stretch effect into the stacked section. In this study, we use spectral shaping to correct for the stretch effect in the VSP-CDP mapped image. We can equalize the spectra of wavelets in the VSP-CDP mapped section by applying spectral shaping, and the reduction of the stretch effect in the unstacked data improves the uniformity of the S/N ratio and the resolution in the stacked data.

**ACKNOWLEDGEMENTS**

ProMAX seismic processing software was provided under a Strategic Partnership with Landmark Graphics. The authors also thank the sponsors of the Berkeley center for reservoir imaging.

**REFERENCES**


Brown, R., 1994. Image quality depends on your point of view. The Leading Edge, 13, No. 6: 669-673.

Harris, J.M., Nolen-Hoeksema, R.C., Langan, R.T., van Schaack, M., Lazaratos, S.K. and Rector, J.W., 1995. High-resolution crosswell imaging of a west Texas carbonate reservoir: Part 1. Project summary and interpretation. Geophysics, 60, No. 3: 667-681.

Haldorsen, J.B.U. and Farmer, P.A., 1989. Resolution and NMO-stretch: imaging by stacking. Geophysical Prospecting, 37: 479-492.

Langan, R.T., Lazaratos, S.K., Harris, J.M., Vassiliou, A.A., Jensen, T.L., Fairborn, J.W., 1998. Crosswell seismic imaging in the Buena Vista Hills, San Joaquin Valley: A case history. Expanded Abstr., 68th Ann. Internat. SEG Mtg., New Orleans: 353-356.

Lazaratos, S.K., 1993. Crosswell Reflection Imaging. Ph.D. Thesis, Stanford Univ. Stanford, CA.

Mo, Le-Wei and Harris, J.M., 1993. Migration of crosswell seismic data. Expanded Abstr., 63rd Ann. Internat. SEG Mtg., Washington, D.C.: 317-320.

Qin, F. and Schuster, G.T., 1993. Constrained Kirchhoff migration of crosswell seismic data. Expanded Abstr., 63rd Ann. Internat. SEG Mtg., Washington, D.C.: 99-102.

Sheline, H.E., 1995. Cross Well Seismic Reservoir Charaterization – a Case Story. Expanded Abstr., 57th Ann. Internat. EAEG Mtg., Session:B049.

Sheriff, R.E., 1991. Encyclopedic Dictionary of Exploration Geophysics. Society of Exploration Geophysicists. Tulsa, OK.

Table 1. Modeling method and velocity pairs used for each problem

| PROBLEM | BASIC THEORY OF THE METHOD USED IN MODELING | VELOCITY PAIR (TOP LAYER / BOTTOM LAYER) |
|---|---|---|
| Phase shift at post-critical incidence angles | Ray tracing | 6000 / 8000 ft/s |
| Fresnel zone effect | Finite difference method (acoustic wave equation) | 6000 / 5900 ft/s |
| Wave stretch in image | Ray tracing | 6000 / 4000 ft/s |

Fig. 1. Model geometry and reflection ray paths for a common source gather with a source located at depth of 2300 ft.

Fig. 2. The effect of the post-critical incidence angle in a common-source gather.

Fig. 3. The effect of the post-critical incidence angle in a common-reflection-point gather.

Fig. 4. The basic geometry for the in-plane Fresnel zone.

Fig. 5. The size of the in-plane Fresnel zone as a function of incidence angle, where $X_F$ is the size of the in-plane Fresnel zone, $X_{well}$ is the distance between source and receiver wells, and X is the horizontal location of the reflection point from the source well (taken from Lazaratos (1993)).

Fig. 6. The effect of the in-plane Fresnel zone in a common-reflection-point gather.

Fig. 7. The image stretch after VSP-CDP mapping in a common-reflection-point gather.

Fig. 8. The stretch effect in the traces stacked with a various incidence angle ranges.

Fig. 9. The spectra of the traces in Fig. 8.

Fig. 10. (a) The wavenumber band of the wavelet for different incidence angles after applying VSP-CDP mapping to the wavelet having a frequency band of 400 ~ 700 Hz in the time domain.

(b) Stacking fold for each wavenumber component of the stacked trace.

Fig. 11. Result after applying spectral shaping to the section in Fig. 7.

Fig. 1.

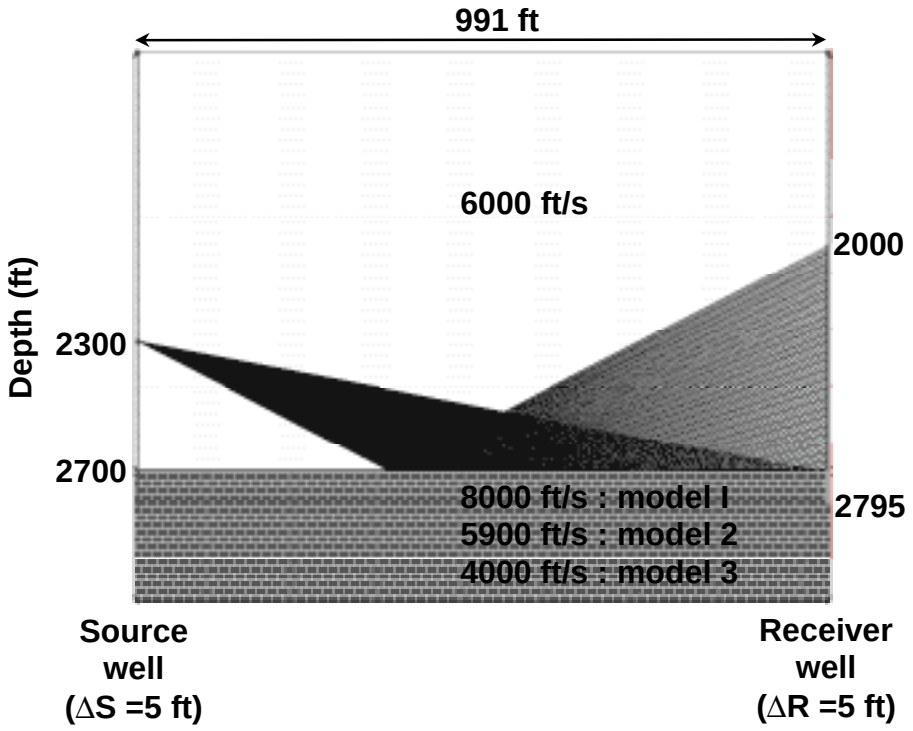
991 ft
6000 ft/s
2000
Depth (ft)
2300
2700
8000 ft/s : model I
5900 ft/s : model 2
4000 ft/s : model 3
2795
Source
well
(ΔS =5 ft)
Receiver
well
(ΔR =5 ft)

Fig. 2.

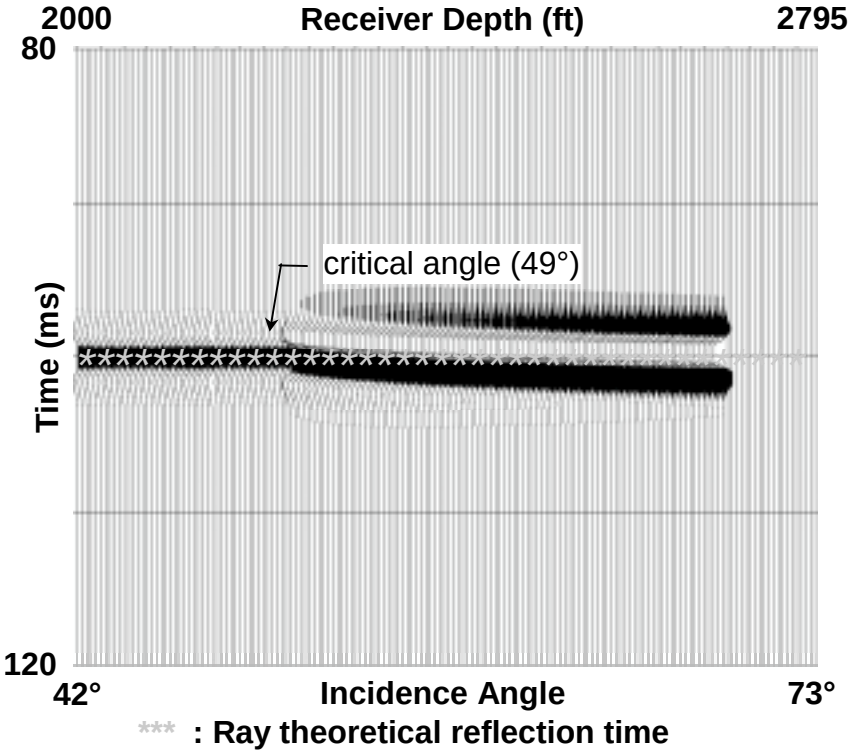
2000
Receiver Depth (ft)
2795
80
critical angle (49°)
Time (ms)
120
42°
Incidence Angle
73°
*** : Ray theoretical reflection time

Fig. 3.

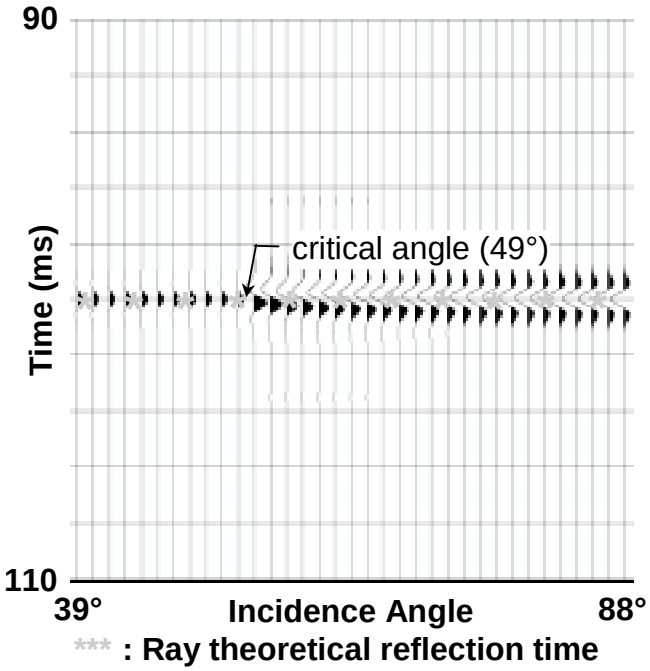
90
Time (ms)
critical angle (49°)
110
39°
Incidence Angle
88°
*** : Ray theoretical reflection time

Fig. 4.

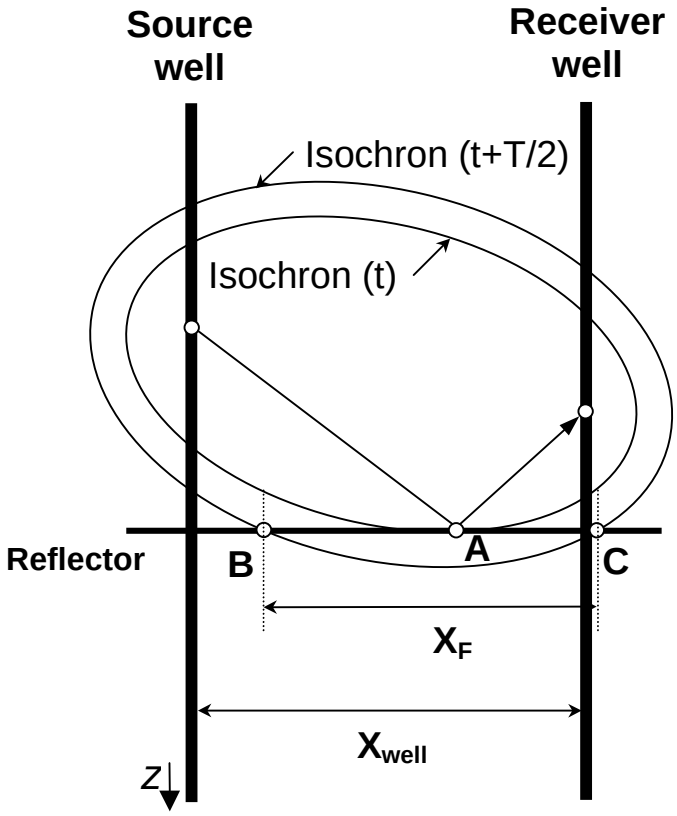
Source well
Receiver well
Isochron (t+T/2)
Isochron (t)
Reflector
B
A
C
$X_F$
$X_{well}$
Z

Fig. 5.

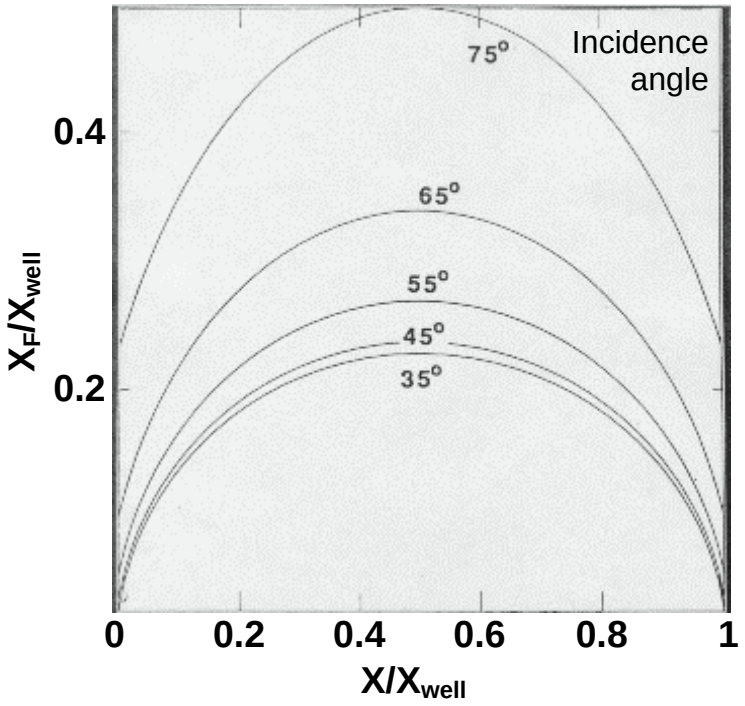
Incidence
angle
75°
65°
55°
45°
35°
0.4
0.2
$X_F/X_{well}$
0
0.2
0.4
0.6
0.8
1
$X/X_{well}$

Fig. 6.

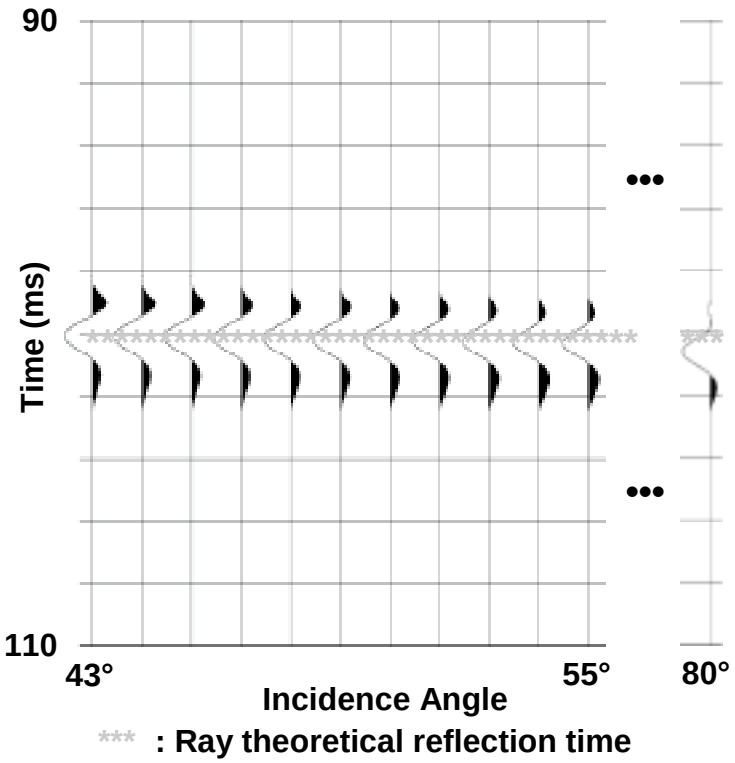
90
110
Time (ms)
43°
55°
80°
Incidence Angle
*** : Ray theoretical reflection time

Fig. 7.

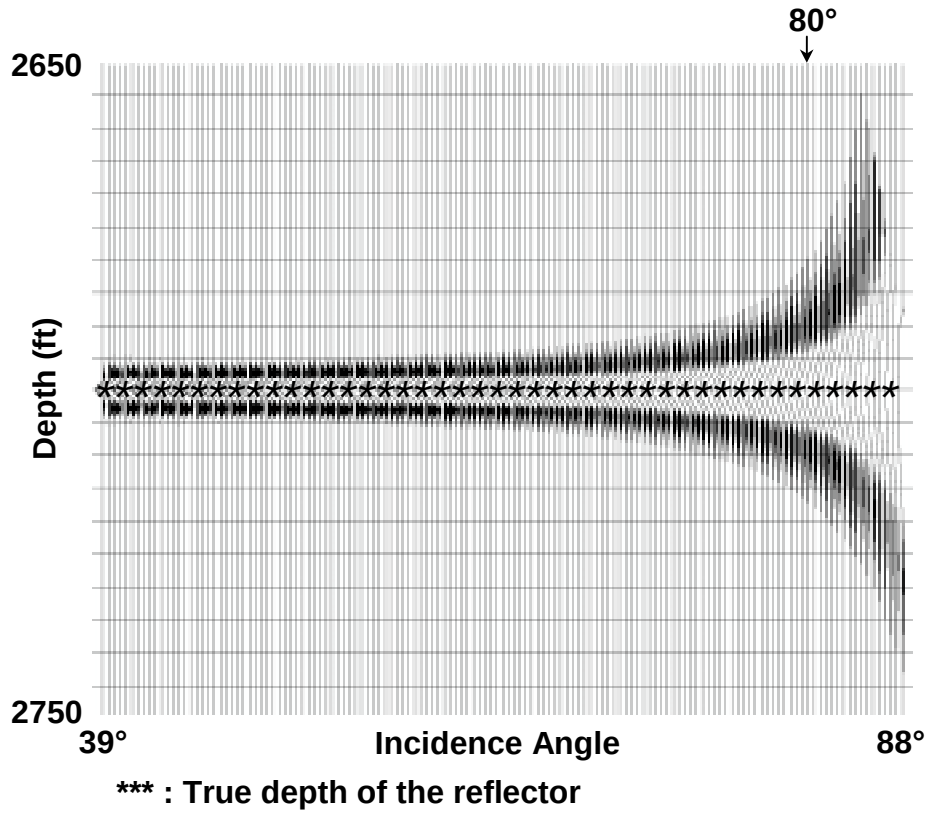
80°
2650
Depth (ft)
2750
39°
Incidence Angle
88°
*** : True depth of the reflector

Fig. 8.

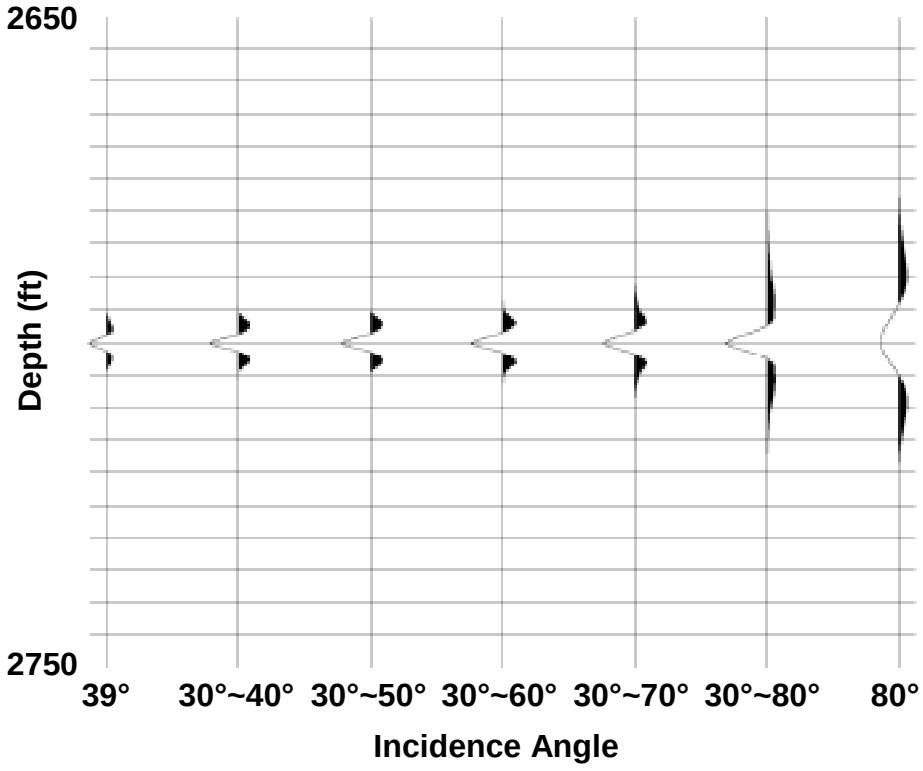
2650
Depth (ft)
2750
39°
30°~40°
30°~50°
30°~60°
30°~70°
30°~80°
80°
Incidence Angle

Fig. 9.

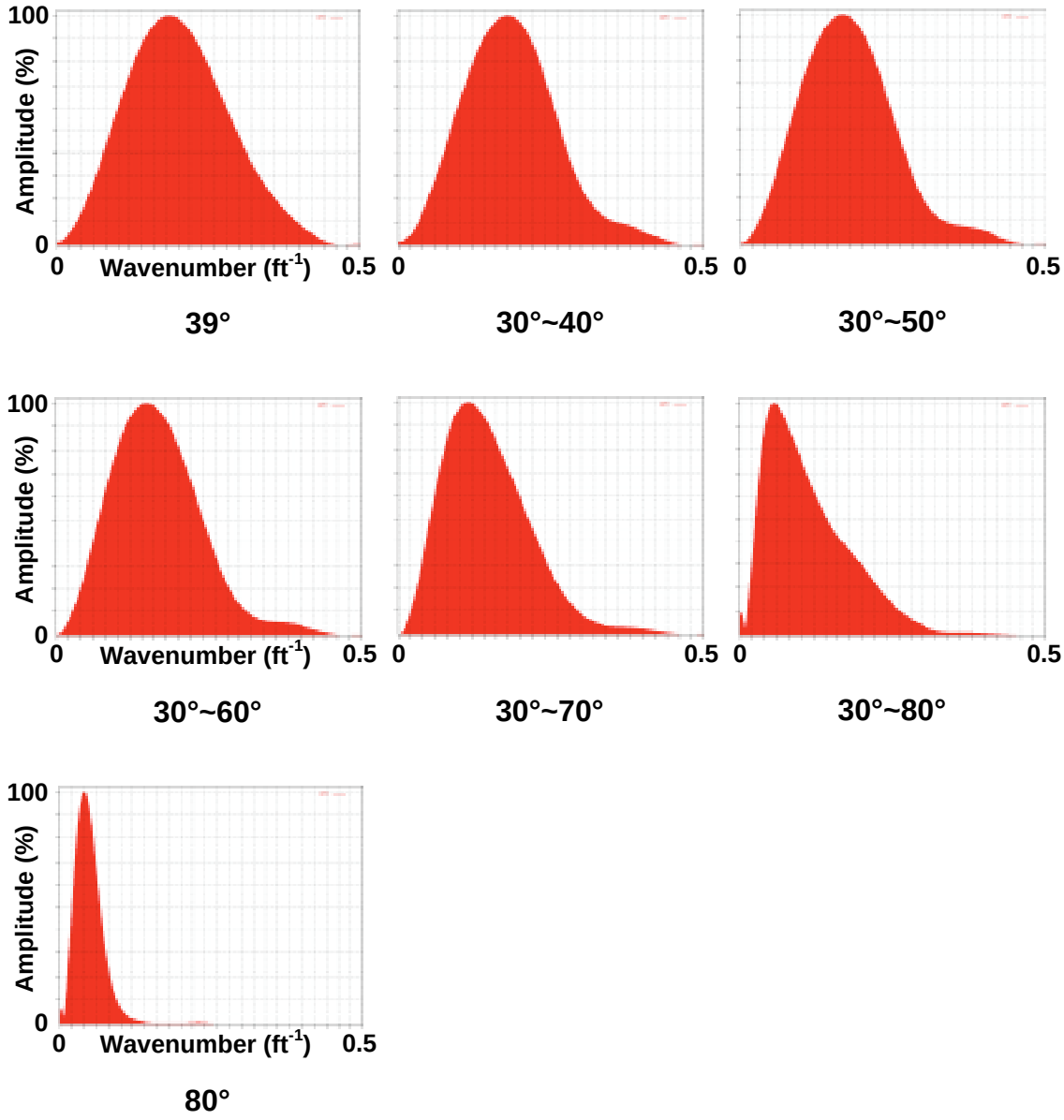
100
Amplitude (%)
0
0
Wavenumber (ft-1)
0.5
39°
30°~40°
30°~50°
30°~60°
30°~70°
30°~80°
80°

Fig. 10.

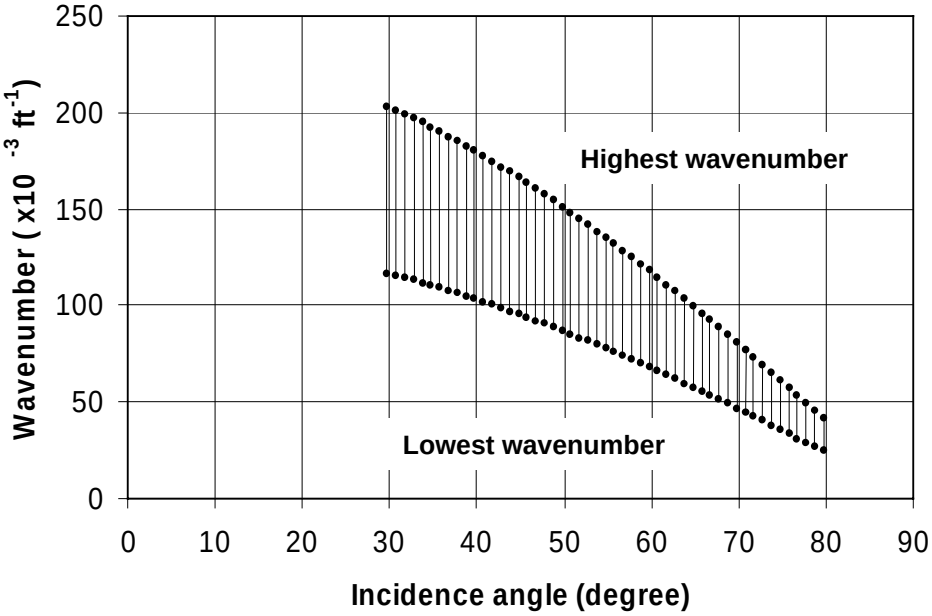
Wavenumber ( x10 -3 ft-1)
250
200
150
100
50
0
Highest wavenumber
Lowest wavenumber
0
10
20
30
40
50
60
70
80
90
Incidence angle (degree)

(a)

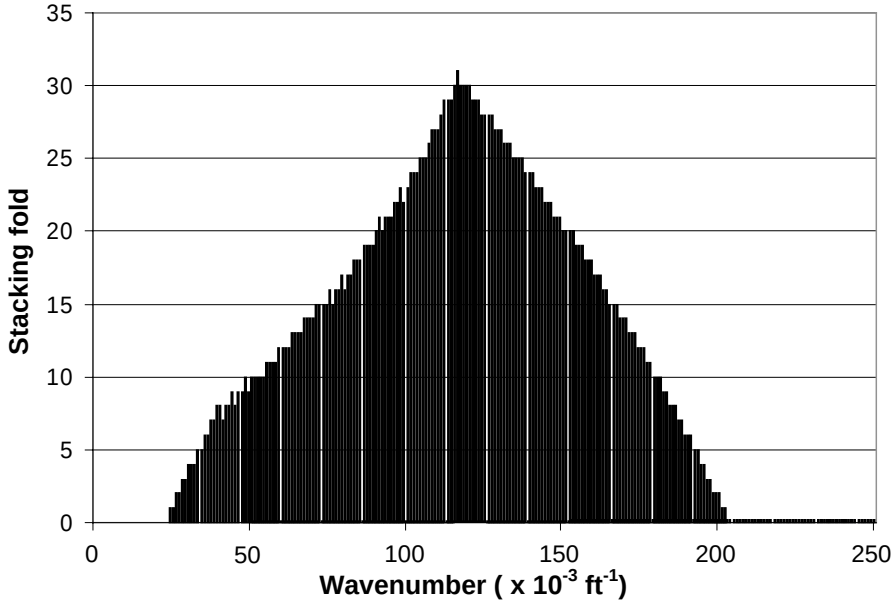
Stacking fold
35
30
25
20
15
10
5
0
0
50
100
150
200
250
Wavenumber ( x 10-3 ft-1)

(b)

Fig. 11.

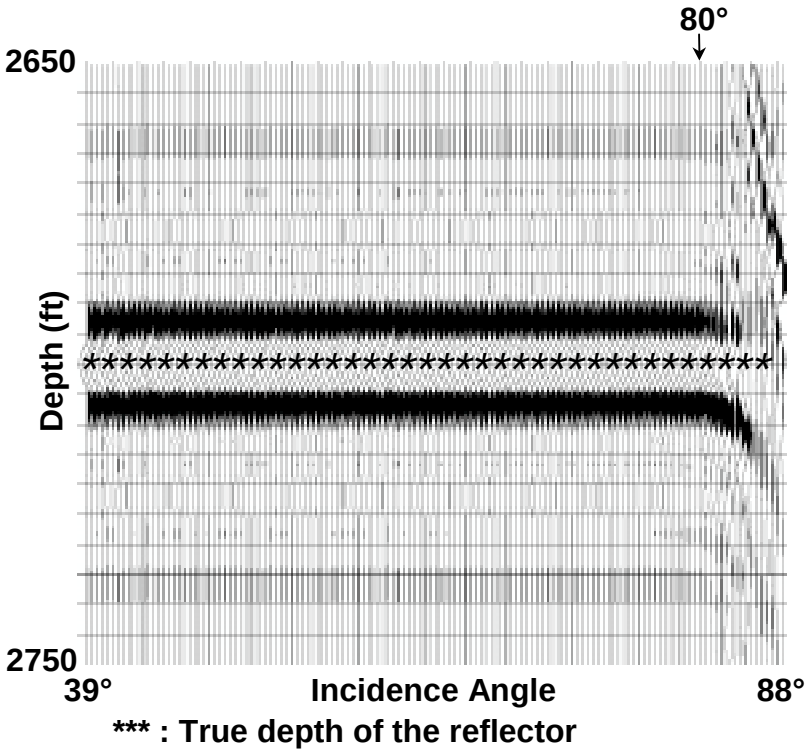
80°
2650
Depth (ft)
2750
39°
Incidence Angle
88°
*** : True depth of the reflector